Digital Signal Processing 78 (2018) 30–41

Contents lists available at ScienceDirect

Digital Signal Processing

www.elsevier.com/locate/dsp

Stokes parameters and 2-D DOAs estimation of polarized sources with an L-shaped coprime array ☆

Wen-xiu Chang *, Xin-bo Li, Jun Wang

College of Communication Engineering, Jilin University, Changchun, Jilin, 130025, China

ARTICLE INFO

Article history:
Available online 1 March 2018

Keywords:
Polarized signal processing
Stokes parameters and 2-D DOAs estimation
L-shaped coprime array
Sparse reconstruction approach

ABSTRACT

In this paper, a sparse reconstruction based approach to estimate Stokes parameters and 2-D DOAs of polarized sources is proposed in case of unknown number of sources. An L-shaped coprime array composed of dipole-dipole pairs, where a dipole in the dipole-dipole pair is placed on x-axis and the other is placed on z-axis, is used to reduce the mutual coupling across two dipoles in the dipole-dipole pair. In order to estimate the elevation of polarized sources, an orthogonal matching pursuit algorithm with the identification of the sources' number (OMP-isn) is proposed. In our proposed approach, the quasi deterministic maximum likelihood (qDML) test step is added in each iteration of algorithm. In addition, a refining grid step is also added in each iteration to reduce the estimation error incurred by the grid mismatch. The OMP algorithm and sparse iterative covariance-based estimation (SPICE) method are employed to estimate the azimuth of polarized sources. In order to pari the azimuth with the elevation, a pair-matching method is proposed based on the l_2-norm and l_1-norm (l_2/l_1) minimization. Based on the pairing azimuth and elevation, Stokes parameters of polarized sources are estimated by using Least Squares (LS) or Total Least Squares (TLS). The stochastic CRB is derived for the 2-D DOAs and Stokes parameters of polarized sources. Simulations are used to verify the performance of the proposed approach.

1. Introduction

Many approaches for estimating the polarization state and DOA of electromagnetic (EM) waves, based on a polarization sensitive array, have been developed [1–18]. By using a dipole-dipole pair, or a loop-loop pair of various orientations, for example, the polarization and DOA estimation of completely polarized (CP) waves were provided in [13] and [15], and the DOA estimation of partially polarized (PP) waves was respectively proposed in [16] and [17]. However, the mutual coupling across two antennas in the dipole-dipole pair or loop-loop pair can result in the fall of the estimate performance for the above approaches [19].

The problem of estimating the two-dimensional (2-D) DOAs (i.e., elevation and azimuth) of multiple incident sources is more important in many application scenarios of array processing. Comparing with the 1-D DOA estimation, the computational complexity of 2-D DOA estimation is very expensive. Thus, many computational efficient estimation algorithms were proposed [20–23]. An oblique projection based approach for the 2-D DOAs estimation of the mixed signals was proposed in [20]. Since the 2-D DOAs estimation is decoupled into two 1-D estimation problems, the computational complexity is reduced. Since the L-shaped array is proved to have a better performance and moderate computational complexity compared with uniform rectangle array or uniform circular array, a 2-D DOAs estimation method was proposed using an L-shaped array in [21]. But, the knowledge of the source number is essential for these methods to work efficiently. In case of unknown number of sources and using an L-shaped array, an interlaced double-precision 2-D angle estimation algorithm was proposed in [22]. However, this algorithm is not used to estimate the polarization state of polarized sources.

Polarization can be described using four parameters known as "Stokes parameters". Stokes parameters are usually arranged in a 4×1 vector called a "Stokes vector". The polarization state of any EM waves, which may be a CP wave, a PP or an unpolarized (UP) wave, can be determined by measuring all four parameters of its Stokes vector. In addition, several useful quantitative measures, such as the degree of polarization, the degree of linear polarization, the degree of circular polarization and so on, can also be calculated from Stokes parameters [24]. In general, Stokes parameters and their derived norms provide a set of tools for the Earth-

☆ This work was supported by the National Natural Science Foundation of China under Grants 61571462.

* Corresponding author.
E-mail address: 732410427@qq.com (W.-x. Chang).

https://doi.org/10.1016/j.dsp.2018.02.016
1051-2004/

observation Remote Sensing, Radio and Radar Astronomy communities. For example, WindSat demonstrated the use of the third Stokes parameter to indicate wind direction [25]. Therefore, it is of theoretical interest and practical importance to develop approaches of estimating Stokes parameters. Unfortunately, the study for estimating Stokes parameters has received a little attention [26].

In this paper, a sparse representation based algorithm to estimate Stokes parameters and 2-D DOAs of polarized sources is considered using an L-shaped coprime array composed of dipole-dipole pairs, in case of unknown number of sources. The coprime arrays have an important advantage over uniform linear arrays (ULAs): it can offer a higher number of degrees-of-freedom (DOFs) for source estimation and reduce the mutual coupling among the antennas [27]. In estimating the elevation of polarized sources, an orthogonal matching pursuit (OMP) algorithm with unknown sparsity level K (or unknown number of sources) is proposed, due to low computational complexity and implementation simplicity of the OMP algorithm. In this algorithm, the quasi deterministic maximum likelihood (qDML) test step is added in each iteration. Unlike the orthogonal matching pursuit with thresholding (OMPT) [28], in which the sparsity level K is not present as stopping term but the choice of threshold parameter requests the knowledge of the sparsity level K, our proposed approach can identify the sparsity level K. In addition, a refining grid step is also added in each iteration to reduce the estimation error incurred by the grid mismatch. The OMP algorithm or sparse iterative covariance-based estimation (SPICE) approach [29,30] are employed to estimate the azimuth of polarized sources in case that the number of sources is previously estimated. In order to pari the azimuth with the elevation, a pair-matching method is proposed based on the l_2-norm and l_1-norm (l_2/l_1) minimization. To improve the performance, Stokes parameters of polarized sources are estimated by using the least squares (LS) or the total least squares (TLS) method. Finally, we derive the stochastic CRB for the 2-D DOAs and Stokes parameters of polarized sources.

The contributions and advantages of the proposed approach are given in the following.

1) The approach proposed in this paper is used to the estimation of Stokes parameters and 2-D DOAs for both the CP and PP sources. It has a broad application.

2) In the proposed approach, the unknown sparsity K is efficiently determined by an identifying step, and the identifying step is included in OMP algorithm. This results in the improvement of OMP algorithm in determining the unknown sparsity K. For many greedy methods, their performance depends on a proper estimation of the unknown sparsity K, denotes by $\hat{K}$. If $\hat{K}$ is less than K, these methods can not recover the K-sparse signal. On the contrary, if $\hat{K}$ is more than K, the efficiency and recovery performance of these methods may degrade. Thus, it is usually very important to determine $\hat{K}$.

3) The computational complexity is decreased by determining the unknown sparsity K. Since the number of sources K is known, the iteration number of OMP is equal to K. When K is unknown, however, the $\lceil 2.8K \rceil$ iterations is at least needed to recover exactly K-sparse signals, where $\lceil 2.8K \rceil$ denotes the nearest integers greater than or equal to $2.8K$ [40]. Thus, the computing cost for the OMP increases heavily along with the increase of the iteration number. Since the unknown sparsity K is efficiently determined, the $K+1$ iterations is only needed for the proposed algorithm in case that the number of sources K is unknown. Because $(K+1) < \lceil 2.8K \rceil$, the computing cost for the proposed algorithm is enormously decreased.

4) The structure used in this paper is not the typical L-shaped array. It is just two components of dipole-dipole pairs placed on x-axis and z-axis at the geometry of coprime array, respectively. The advantage of this structure is to reduce the mutual coupling across

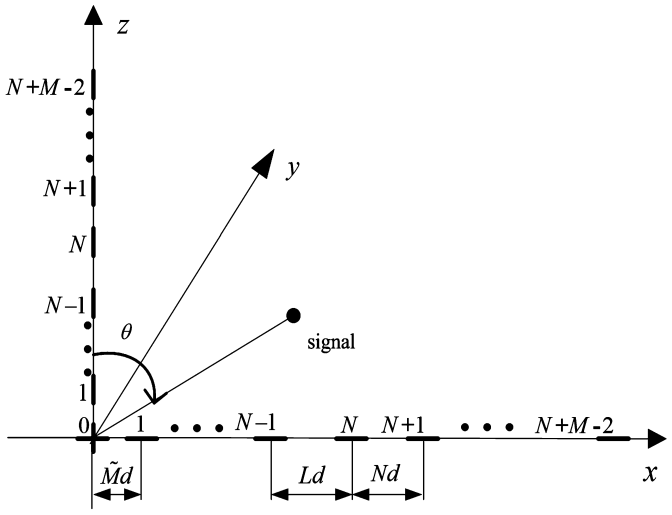

Fig. 1. an L-shaped array with two CADiS.

two dipoles in the dipole-dipole pair. Although the DOA estimation with coprime array has been discussed in many papers, the structure used in this paper is first used to estimate Stokes parameters and 2-D DOAs for both the CP and PP sources.

2. Polarized source model and coprime array

2.1. Polarized source model

Consider a scenario with one narrowband, plane EM wave, which is traveling in an isotropic and homogeneous medium, impinges on an L-shaped coprime array, which consists of two coprime array with $Q = (M + N - 1)$ dipoles along x-axis and z-axis respectively, where M and N are coprime integers, as shown in Fig. 1. By overlooking all mutual coupling among the sensors, we define the components of electric field in x-axis and z-axis as [19], [10]

$$\mathbf{Z}(t) = \begin{bmatrix} z_x(t) \\ z_z(t) \end{bmatrix} = \begin{bmatrix} -\sin\phi & \cos\phi\cos\theta \\ 0 & -\sin\theta \end{bmatrix} \mathbf{E}(t) \tag{1}$$

where $\theta \in [0, \pi]$ and $\phi \in [0, 2\pi)$ denote the incidence source's elevation measured from the positive z axis and azimuth measured from the positive x axis, respectively. $\mathbf{E}(t) = \begin{bmatrix} E_H(t) & E_V(t) \end{bmatrix}^T$ is the electric field of EM wave, where $E_H(t)$ and $E_V(t)$ are the H- and V-components of electric field. It is assumed to be zero-mean complex Gaussian random processes with second-order circularity. Then, the covariance matrix $\mathbf{R}_{EE}$ of $\mathbf{E}(t)$ is given by [16]

$$\begin{aligned} \mathbf{R}_{EE} &= \left\langle \mathbf{E}(t)\mathbf{E}(t)^H \right\rangle = \begin{bmatrix} \langle E_H(t)E_H^*(t)\rangle & \langle E_H(t)E_V^*(t)\rangle \\ \langle E_V(t)E_H^*(t)\rangle & \langle E_V(t)E_V^*(t)\rangle \end{bmatrix} \\ &= \begin{bmatrix} r_{E_H} & r_{E_HE_V} \\ r_{E_HE_V}^* & r_{E_V} \end{bmatrix} \end{aligned} \tag{2}$$

where the symbol $\langle . \rangle$ denotes the expectation operator. Superscripts $(.)^*$ and $(.)^H$ denote complex conjugate and Hermitian operation, respectively. From (2), Stokes parameters of EM wave are given by

$$g_0 = r_{E_H} + r_{E_V} \tag{3}$$

$$g_1 = r_{E_H} - r_{E_V} \tag{4}$$

$$g_2 = 2\Re\{r_{E_HE_V}\} \tag{5}$$

$$g_3 = -2\Im\{r_{E_HE_V}\} \tag{6}$$

where the symbol $\Re\{r_{E_H E_V}\}$ and $\Im\{r_{E_H E_V}\}$ denote the real part and imaginary part of $r_{E_H E_V}$, respectively. Stokes parameters are often used to calculate the power g_0 of an EM wave, and to describe the polarization state and degree of polarization (DP) of an EM wave. The DP can be calculated as

$$DP = \frac{\sqrt{g_1^2 + g_2^2 + g_3^2}}{g_0} \tag{7}$$

where $0 \le DP \le 1$. If an EM wave is completely polarized, $DP = 1$. If an EM wave is unpolarized, $DP = 0$. Moreover, an EM wave is partially polarized when $0 < DP < 1$.

When K uncorrelated, plane EM wave impinge on this coprime array from direction $((\theta_1, \phi_1), \cdots, (\theta_K, \phi_K))$, the data vector measured by the dipoles along x-axis and z-axis at time t is given by

$$\begin{aligned}\mathbf{x}(t) &= \sum_{k=1}^{K} \mathbf{a}(\phi_k) z_{x,k}(t) + \mathbf{n}_x(t) \\ \mathbf{z}(t) &= \sum_{k=1}^{K} \mathbf{a}(\theta_k) z_{z,k}(t) + \mathbf{n}_z(t), \quad t = 1, 2, \cdots, T\end{aligned} \tag{8}$$

where $\mathbf{n}_x(t)$ and $\mathbf{n}_z(t)$ are the additive noise vector, which are assumed to be independent and identically distributed (i.i.d.) random vector following the complex Gaussian distribution $\mathcal{CN}(\mathbf{0}, \sigma_n^2 \mathbf{I})$, and it is uncorrelated with all of source signals. $\mathbf{a}(\phi_k) = [e^{-jd_1\alpha_k}, e^{-jd_2\alpha_k}, \cdots, e^{-jd_Q\alpha_k}]^T$ and $\mathbf{a}(\theta_k) = [e^{-jd_1\beta_k}, e^{-jd_2\beta_k}, \cdots, e^{-jd_Q\beta_k}]^T$, where $\alpha_k = (2\pi/\lambda)\cos(\phi_k)$ and $\beta_k = (2\pi/\lambda)\cos(\theta_k)$, are the spatial phase vector for the kth source, along x-axis and z-axis. λ and d_l $(l = 1, 2, \cdots, Q)$ denote the wavelength and the inter-element spacing relative to the origin. Inserting (1) into (8), we have

$$\begin{aligned}\mathbf{u}(t) &= \begin{bmatrix} \mathbf{x}(t) \\ \mathbf{z}(t) \end{bmatrix} \\ &= \sum_{k=1}^{K} \underbrace{\begin{bmatrix} \mathbf{a}(\phi_k) & 0 \\ 0 & \mathbf{a}(\theta_k) \end{bmatrix}}_{\mathbf{\Lambda}_k} \underbrace{\begin{bmatrix} -\sin\phi_k & \cos\phi_k \cos\theta_k \\ 0 & -\sin\theta_k \end{bmatrix}}_{\mathbf{\Psi}_k} \mathbf{E}_k(t) \\ &\quad + \begin{bmatrix} \mathbf{n}_x(t) \\ \mathbf{n}_z(t) \end{bmatrix}\end{aligned} \tag{9}$$

Next, we can construct the covariance matrix

$$\mathbf{R} = \left\langle \mathbf{u}(t)\mathbf{u}^H(t) \right\rangle = \sum_{k=1}^{K} (\mathbf{\Lambda}_k \mathbf{\Psi}_k) \mathbf{R}_{E_k E_k} (\mathbf{\Lambda}_k \mathbf{\Psi}_k)^H + \mathbf{N} \tag{10}$$

where $\mathbf{R}_{E_k E_k}$ is the covariance matrix of the kth source $\mathbf{E}_k(t)$ and $\mathbf{N} = \sigma_n^2 \mathbf{I}$ is the covariance matrix of additive noise vector.

2.2. Coprime array with displaced subarrays (CADiS)

Consider two collinearly located uniform linear subarrays, as shown in Fig. 1, where one consists of N dipoles and the other with $M-1$ dipoles. We assume N and M are coprime and M can be expressed as a product of two positive integers p and $\tilde{M}$, i.e. $M = p\tilde{M}$. The closest spacing between the two subarrays is set to Ld, where $d = \lambda/2$ and $L \ge min(\tilde{M}, N)$. The array sensors are positioned at

$$\begin{aligned}\mathcal{P} = &\{\tilde{M}nd | 0 \le n \le N-1\} \\ &\cup \{(\tilde{M}(N-1) + L + mN)d | 0 \le m \le M-2\}\end{aligned} \tag{11}$$

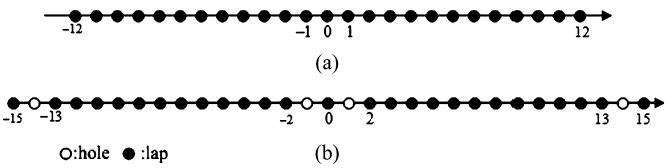

Fig. 2. An example of the difference coarray, where $M = 4$, $N = 3$ and $L = \tilde{M} + N$. (a) $\tilde{M} = 1$; (b) $\tilde{M} = 2$.

From (11), the total array aperture of the CADiS is $(\tilde{M}(N-1) + L + (M-2)N)d = N_{max}d$.

For a CADiS specified by the integer set $\mathcal{P}$, its difference coarray $\mathcal{D}$ is defined as

$$\mathcal{D} = \{n_1 - n_2 | n_1, n_2 \in \mathcal{P}\} \tag{12}$$

The difference coarray consists of the self-differences of two subarrays in the CADiS and their cross-differences. The self-differences in the coarray has positions [27]

$$\mathcal{L}_s = \{l_s | l_s = Nmd\} \cup \{l_s | l_s = \tilde{M}nd\} \tag{13}$$

and the corresponding mirrored position $\mathcal{L}_s^- = \{-l_s | l_s \in \mathcal{L}_s\}$, whereas the cross-differences has positions

$$\mathcal{L}_c = \{l_c | l_c = (\tilde{M}(N-1) + L + mN - \tilde{M}n)d\} \tag{14}$$

and the corresponding mirrored position $\mathcal{L}_c^- = \{-l_c | l_c \in \mathcal{L}_c\}$, where $0 \le n \le N-1$ and $0 \le m \le M-2$. Consequently, the full set of lags in the difference coarray is given by

$$\mathcal{L}_P = \mathcal{L}_s \cup \mathcal{L}_s^- \cup \mathcal{L}_c \cup \mathcal{L}_c^- \tag{15}$$

When $L = \tilde{M} + N$ is a choice, the largest number of consecutive lags is obtained. in this case, there are the maximum number of unique lags $M_m = 2MN + 2\tilde{M} - 1$, among which range $[(\tilde{M}-1)(N-1), MN + \tilde{M} - 1]$ and its corresponding negative range $[-MN - \tilde{M} + 1, -(\tilde{M}-1)(N-1)]$ are respectively consecutive [27]. An example of the difference coarray is shown in Fig. 2, where $M = 4$, $N = 3$ and $L = \tilde{M} + N$. Fig. 2(a) and (b) show the full set of lags in the difference coarray, for $\tilde{M} = 1$ and $\tilde{M} = 2$ respectively. Fig. 2(b) indicates that some "holes", e.g., ± 1, ± 14, still exist in the difference coarray. The total number of lags in the symmetric set gives a global upper bound of the achievable DOFs.

3. Stokes parameters and 2-D DOAs estimation

In order to employ the DOFs offered by the difference coarray, we directly take the vectorization operation on the covariance matrix $\mathbf{R}$. Thus, the following measurement vector is obtained.

$$\mathbf{r} = \mathrm{vec}(\mathbf{R}) = \sum_{k=1}^{K} \mathbf{A}_k \bar{\mathbf{e}}_k + \bar{\mathbf{n}} = \mathbf{A}\bar{\mathbf{e}} + \bar{\mathbf{n}} \tag{16}$$

where $\mathbf{A} = [\mathbf{A}_1, \cdots, \mathbf{A}_K]$, $\bar{\mathbf{e}} = [\bar{\mathbf{e}}_1^T, \cdots, \bar{\mathbf{e}}_K^T]^T$, $\bar{\mathbf{n}} = \mathrm{vec}(\mathbf{N})$, and

$$\mathbf{A}_k = (\mathbf{\Lambda}_k \mathbf{\Psi}_k)^* \otimes (\mathbf{\Lambda}_k \mathbf{\Psi}_k) = \underbrace{(\mathbf{\Lambda}_k^* \otimes \mathbf{\Lambda}_k)}_{\bar{\mathbf{\Lambda}}_k} \underbrace{(\mathbf{\Psi}_k^* \otimes \mathbf{\Psi}_k)}_{\bar{\mathbf{\Psi}}_k} \tag{17}$$

$$\bar{\mathbf{\Lambda}}_k = \begin{bmatrix} \mathbf{a}^*(\phi_k) \otimes \mathbf{a}(\phi_k) & 0 & 0 & 0 \\ 0 & \mathbf{a}^*(\phi_k) \otimes \mathbf{a}(\theta_k) & 0 & 0 \\ 0 & 0 & \mathbf{a}^*(\theta_k) \otimes \mathbf{a}(\phi_k) & 0 \\ 0 & 0 & 0 & \mathbf{a}^*(\theta_k) \otimes \mathbf{a}(\theta_k) \end{bmatrix} \tag{18}$$

$$\bar{\mathbf{\Psi}}_k = \begin{bmatrix} \sin^2\phi_k & -\sin\phi_k \cos\phi_k \cos\theta_k & -\sin\phi_k \cos\phi_k \cos\theta_k & \cos^2\phi_k \cos^2\theta_k \\ 0 & \sin\phi_k \sin\theta_k & 0 & -\sin\theta_k \cos\phi_k \cos\theta_k \\ 0 & 0 & \sin\phi_k \sin\theta_k & -\sin\theta_k \cos\phi_k \cos\theta_k \\ 0 & 0 & 0 & \sin^2\theta_k \end{bmatrix} \tag{19}$$

$$\bar{\mathbf{e}}_k = \mathrm{vec}(\mathbf{R}_{E_k E_k}) = \underbrace{\begin{bmatrix} 1/2 & 1/2 & 0 & 0 \\ 0 & 0 & 1/2 & j/2 \\ 0 & 0 & 1/2 & -j/2 \\ 1/2 & -1/2 & 0 & 0 \end{bmatrix}}_{\mathbf{J}} \begin{bmatrix} g_{0,k} \\ g_{1,k} \\ g_{2,k} \\ g_{3,k} \end{bmatrix} = \mathbf{J}\bar{\mathbf{g}}_k \tag{20}$$

where $\otimes$ denotes the Kronecker product. Our interest is to estimate the 2-D DOAs and Stokes parameters of the received polarized sources from the observed data samples, in case of unknown number of sources.

3.1. Estimation of the elevation

In the $4Q^2 \times 1$ measurement vector $\mathbf{r}$, we take the final Q^2 rows (i.e. the vectorization operation on the covariance matrix $\mathbf{R}_z = \left\langle \mathbf{z}(t)\mathbf{z}^H(t) \right\rangle$) as a measurement vector $\mathbf{r}_z$. From (16), we have

$$\mathbf{r}_z = \sum_{k=1}^{K} (\mathbf{a}^*(\theta_k) \otimes \mathbf{a}(\theta_k)) p_k + \bar{\mathbf{n}}_z = \mathbf{F}\mathbf{p} + \bar{\mathbf{n}}_z \tag{21}$$

where $\mathbf{p} = [p_1, \cdots, p_K]^T$ with $p_k = \frac{1}{2}\sin^2\theta_k(g_{0,k} - g_{1,k})$, $\bar{\mathbf{n}}_z$ is the final Q^2 rows of vector $\bar{\mathbf{n}}$ and $\mathbf{a}^*(\theta_k) \otimes \mathbf{a}(\theta_k)$ is the spatial phase vector of the kth source for the difference coarray along z-axis, which has elements $a_{l_1,l_2} = e^{jd_{l_1}\beta_k} e^{-jd_{l_2}\beta_k} = exp(j\underbrace{(d_{l_1} - d_{l_2})}_{\triangle_{l_1,l_2} d}\beta_k)$ where $l_1, l_2 \in Q$. Because $\triangle_{l_1,l_2} \in \mathcal{L}_P$, the vector $\mathbf{r}_z$ can be regard as a data received from the difference coarray along z-axis, whose corresponding steering matrix is defined by $\mathbf{F} = [(\mathbf{a}^*(\theta_1) \otimes \mathbf{a}(\theta_1)), \cdots, (\mathbf{a}^*(\theta_K) \otimes \mathbf{a}(\theta_K))]$.

By discretizing the range of interest as a uniform grid $\mathbf{\Theta} = (\theta_1, \cdots, \theta_D)$ with spacing $\Delta\theta$, the model in equation (21) can be transformed into

$$\mathbf{r}_z = \mathbf{F}(\mathbf{\Theta})\tilde{\mathbf{p}} + \bar{\mathbf{n}}_z \tag{22}$$

where $\tilde{\mathbf{p}}$ is a sparse vector with the unknown sparse level K. We have $\tilde{\mathbf{p}}_i$ is nonzero if the kth source is located at θ_i, otherwise $\tilde{\mathbf{p}}_i$ is zero. In this paper, we assume that two targets are at least $\Delta\theta$ apart, i.e., $|\theta_i - \theta_j| \geq \Delta\theta$ for all $1 \leq i, j \leq K$.

By employing the OMP algorithm, the support of a sparse vector (index set of nonzero elements) can be recovered from the measurements $\mathbf{r}_z$ under some recovery conditions. Thus, the elevation $(\hat{\theta}_1, \cdots, \hat{\theta}_K)$ can be estimated using the index set of nonzero elements. The OMP algorithm is an iterative algorithm. The number of iterations is typically set to the sparsity level K of the sparse vector to be recovered. However, the sparsity level K is unknown due to unknown number of sources. In case that the sparsity level K is unknown, more iterations than the sparsity level K must be adopted. This results in more indices than the sparsity level K. To select the indices corresponding with the true elevation of received sources from candidates in the index set, an identifying step is added in OMP algorithm.

In the identifying step, we use the orthogonal projection criterion to find the number of the received polarized sources. At each iteration, we form the Vandermonde matrix using the estimated elevation corresponding with all indices in the index set. At the kth iteration, for example, the Vandermonde matrix $\hat{\mathbf{F}}(\mathbf{\Theta}_k)$ can be written by the estimated elevation $\mathbf{\Theta}_k = (\hat{\theta}_1, \cdots, \hat{\theta}_k)$. Then we defined a cost function

$$L_{qDML}(\mathbf{\Theta}_k) = |\mathbf{P}_{\hat{\mathbf{F}}(\mathbf{\Theta}_k)}\mathbf{r}_z|^2 \tag{23}$$

where the symbol $|\ |$ denotes the magnitude of a vector, and

$$\mathbf{P}_{\hat{\mathbf{F}}(\mathbf{\Theta}_k)} = \hat{\mathbf{F}}(\mathbf{\Theta}_k)(\hat{\mathbf{F}}^H(\mathbf{\Theta}_k)\hat{\mathbf{F}}(\mathbf{\Theta}_k))^{-1}\hat{\mathbf{F}}^H(\mathbf{\Theta}_k) \tag{24}$$

In fact, $|\mathbf{P}_{\hat{\mathbf{F}}(\mathbf{\Theta}_k)}\mathbf{r}_z|^2 = \|\mathbf{P}_{\hat{\mathbf{F}}(\mathbf{\Theta}_k)}\mathbf{r}_z\|_2^2$, where the symbol $\|\ \|_2$ denotes the Euclidean norm. The geometric interpretation of the cost function (23) is the following. The signal component of $\mathbf{r}_z$ always lies in the signal subspace defined by the columns of $\mathbf{F}(\mathbf{\Theta}_K)$. The noise has two effects; it adds noise into the signal subspace and it adds noise in an orthogonal space that causes $\mathbf{r}_z$ to lie outside the signal subspace. To find the K steering vectors that form a signal subspace that is as close as possible to the $\mathbf{r}_z$, the cost function (23) is used. The cost function (23) represents the magnitude of the projection of vector $\mathbf{r}_z$ onto the estimated signal subspace. By the cost function (23), closeness between the signal subspace and the vector $\mathbf{r}_z$ can be measured. In fashion of equation, the cost function (23) is similar to the DML cost function [39]. Thus, it is referred to the quasi DML cost function.

If the differential coefficient $\triangle l_k = L_{qDML}(\mathbf{\Theta}_k) - L_{qDML}(\mathbf{\Theta}_{k-1}) < \varepsilon_k$, the iteration stops. The iterative number $k-1$ is the estimation of the number of sources. Since this algorithm can identify the number of the received sources, it is referred to the OMP with the identification of the sources' number (OMP-isn).

Next, we clarify how to choose the threshold ε_k. Consider the partition of the vector $\mathbf{r}_z$ into its components in the signal and noise subspace

$$\mathbf{r}_z = \mathbf{T}\begin{bmatrix} \mathbf{r}_s \\ \mathbf{r}_n \end{bmatrix} \tag{25}$$

where $\mathbf{r}_s$ denotes the $k \times 1$ component in the signal subspace, $\mathbf{r}_n$ denotes the component in the noise subspace, and $\mathbf{T}$ denotes a unitary coordinate transformation matrix. Thus, the vector $\mathbf{r}_z$ satisfies the relations

$$\mathbf{P}_{\hat{\mathbf{F}}(\mathbf{\Theta}_k)}\mathbf{r}_z = \mathbf{T}\begin{bmatrix} \mathbf{r}_s \\ \mathbf{0} \end{bmatrix} \tag{26}$$

By Equation (26), we have

$$\mathbf{P}_{\hat{\mathbf{F}}(\mathbf{\Theta}_k)}\mathbf{R}_r\mathbf{P}_{\hat{\mathbf{F}}(\mathbf{\Theta}_k)} = \mathbf{T}\begin{bmatrix} \mathbf{R}_s & \mathbf{0} \\ \mathbf{0} & \mathbf{0} \end{bmatrix}\mathbf{T}^H \tag{27}$$

where $\mathbf{R}_r$ is the covariance matrix of $\mathbf{r}_z$ and $\mathbf{R}_s$ is the covariance matrix of $\mathbf{r}_s$. By the invariance of the trace under the transformation $\mathbf{R} \longrightarrow \mathbf{T}\mathbf{R}\mathbf{T}^H$, with $\mathbf{T}$ unitary, implies that

$$\begin{aligned} L_{qDML}(\mathbf{\Theta}_k) &= |\mathbf{P}_{\hat{\mathbf{F}}(\mathbf{\Theta}_k)}\mathbf{r}_z|^2 = tr[\mathbf{P}_{\hat{\mathbf{F}}(\mathbf{\Theta}_k)}\mathbf{R}_r\mathbf{P}_{\hat{\mathbf{F}}(\mathbf{\Theta}_k)}] \\ &= tr[\mathbf{R}_s] = \sum_{i=1}^{k} l_i \end{aligned} \tag{28}$$

where l_i denotes the ith eigenvalue of $\mathbf{R}_s$. Since $l_i > 0$, $L_{qDML}(\mathbf{\Theta}_k)$ increases monotonously along with increase of k. Based on monotonicity and nondecreasing of $L_{qDML}(\mathbf{\Theta}_k)$, there is only one minimum l_1 at $k = 1$. From (28), we have the differential coefficient $\triangle l_k = \sum_{i=1}^{k} l_i - \sum_{i=1}^{k-1} l_i = l_k$ where l_k is the kth eigenvalue of $\mathbf{R}_s$. When the iterative number k is less than the number of sources K, $L_{qDML}(\mathbf{\Theta}_k)$ increases quickly and the differential coefficient $\triangle l_k$ has larger value because l_k $(k = 1, \cdots, K)$ belongs to the signal subspace and has big value. When $k > K$, however, $L_{qDML}(\mathbf{\Theta}_k)$ increases slowly and the differential coefficient $\triangle l_k$ has less value. The reason is that l_k at $k > K$ belongs to the noise subspace and has small value. Since $\triangle l_k = l_k = p_k^2 = \frac{1}{4}\sin^4\theta_k(g_{0,k} - g_{1,k})^2$ at $k \leq K$, we chose the parameter $\varepsilon_k = \varepsilon_0(\sin^4\theta_k)$, where $\varepsilon_0 \leq min\{\frac{1}{4}(g_{0,k} - g_{1,k})^2, k = 1, \cdots, K\}$. If we select a threshold ε_0, let $\triangle l_k > \varepsilon_k$ when $k \leq K$, and $\triangle l_k \leq \varepsilon_k$ when $k = K + 1$. Thus, we can select $\triangle l_k \leq \varepsilon_k$ as the condition ending iteration. In practice, ε_0 can be estimated by the eigenvalues of the covariance matrix $\mathbf{R}_r = \mathbf{r}_z\mathbf{r}_z^H$.

Table 1
The OMP-isn algorithm with the refining grid step.

Input	measurements $\mathbf{r}_z$; measurement matrix $\mathbf{F}_r$ (with δ_r) and $\mathbf{F}_f$ (with δ_f); fine grid set $\mathbf{\Theta}_f$; max sparsity level K_m; threshold ε_0
Initialize	iteration counter $k=0$; estimated index set $T=\emptyset$; residual vector $\mathbf{y}^0=\mathbf{r}_z$; $\mathbf{\Theta_0}=\emptyset$; $l^0=-\varepsilon_0$
While	$k<K_m$ **do**
	$k=k+1$
	$t_r=arg\underbrace{max}_{i}\|\mathbf{F}_r^H[i]\mathbf{y}^{k-1}\|_2$
	$t_f=arg\underbrace{max}_{i\in\Gamma}\|\mathbf{F}_f^H[i]\mathbf{y}^{k-1}\|_2$, where $\Gamma=[t_r-2\delta_r,t_r+2\delta_r]$;
	$t=\frac{\delta_r}{\delta_f}(t_r-2\delta_r)+t_f$
	$\mathbf{\Theta}_k=\mathbf{\Theta}_{k-1}\cup\hat{\theta}_t$, where θ_t is the tth element in $\mathbf{\Theta}_f$
	$\mathbf{P}_{\hat{\mathbf{F}}(\mathbf{\Theta}_k)}=\hat{\mathbf{F}}(\mathbf{\Theta}_k)(\hat{\mathbf{F}}^H(\mathbf{\Theta}_k)\hat{\mathbf{F}}(\mathbf{\Theta}_k))^{-1}\hat{\mathbf{F}}^H(\mathbf{\Theta}_k)$
	$l^k=\|\mathbf{P}_{\hat{\mathbf{F}}(\mathbf{\Theta}_k)}\mathbf{r}_z\|^2$
	$\triangle l_k=l^k-l^{k-1}$
	if $\varepsilon_k=\varepsilon_0 sin^4(\hat{\theta}_t)$
	if $\triangle l_k\geq\varepsilon_k$
	$T=T\cup t$
	$\mathbf{x}=argmin\|\mathbf{r}_z-\sum_{i\in T}\mathbf{F}_f[i]\mathbf{u}\|_2$
	$\mathbf{y}^k=\mathbf{r}_z-\sum_{i\in T}\mathbf{F}_f[i]\mathbf{x}$
	else $k=K_m+1$
	end
End while	
Output	the estimated index set T and vector $\mathbf{x}$

In our OMP-isn algorithm, it is required neither to find the maximum of the quasi DML cost function, nor to find the minimum of the differential coefficient. The OMP-isn algorithm is convergent as long as a suitable threshold ε_0 is selected.

In real applications, there are some cases that the locations of sources do not fall on the predefined grid. This results in grid mismatches and the performance of sparse-based estimator is deteriorated. Inspired by the idea of adaptive grid refinement [31], we add a refining grid step to the OMP-isn algorithm to reduce the effects of grid mismatches. In our framework, we create two uniform grid by discretizing the range of interest, i.e. a rough grid $\mathbf{\Theta}_r$ with spacing δ_r and a fine grid $\mathbf{\Theta}_f$ with spacing δ_f, where $\delta_f=\delta_r/\tau$. In general, the rough grid should not be too rough to achieve better precision and the fine grid should not be too fine to reduce computational complexity and the correlation between the columns of dictionary matrix. $\delta_r=1^\circ$ and $\delta_f=0.1^\circ$ are selected in this paper. In the refining grid step of the OMP-isn algorithm, we use firstly the dictionary matrix formed by rough grid to get the index t_r. Around t_r, we pick an interval $\Gamma=[t_r-2\delta_r,t_r+2\delta_r]$. Then, we use the dictionary matrix formed by fine grid to get the index t_f in the interval Γ. See Table 1 for a detailed description of the OMP-isn algorithm with the refining grid step. In Table 1, the symbol $[i]$ denotes the ith row for a matrix.

3.2. Estimation of the azimuth

In the $4Q^2\times 1$ measurement vector $\mathbf{r}$, we take the first Q^2 rows (i.e. the vectorization operation on the covariance matrix $\mathbf{R}_x=\left(\mathbf{x}(t)\mathbf{x}^H(t)\right)$) as a measurement vector $\mathbf{r}_x$. From (16), we have

$$\mathbf{r}_x=\sum_{k=1}^{K}(\mathbf{a}^*(\phi_k)\otimes\mathbf{a}(\phi_k))q_k+\bar{\mathbf{n}}_x=\mathbf{G}\mathbf{q}+\bar{\mathbf{n}}_x \tag{29}$$

where $\mathbf{q}=[q_1,\cdots,q_K]^T$ with

$$q_k=\frac{1}{2}\sin^2\phi_k(g_{0,k}+g_{1,k})+\frac{1}{2}\cos^2\phi_k\cos^2\theta_k(g_{0,k}-g_{1,k})-(\sin\phi_k\cos\phi_k\cos\theta_k)g_{2,k}$$

$\bar{\mathbf{n}}_x$ is first Q^2 rows of vector $\bar{\mathbf{n}}$ and $\mathbf{a}^*(\phi_k)\otimes\mathbf{a}(\phi_k)$ is the spatial phase vector of the kth source for the difference coarray along x-axis, which has elements $a_{l_1,l_2}=e^{jd_{l_1}\alpha_k}e^{-jd_{l_2}\alpha_k}=exp(j\underbrace{(d_{l_1}-d_{l_2})}_{\triangle_{l_1,l_2}d}\alpha_k)$ where $l_1,l_2\in Q$. Because $\triangle_{l_1,l_2}\in\mathcal{L}_P$, the vector $\mathbf{r}_x$ can be regard as a data vector received from the difference coarray along x-axis, whose corresponding steering matrix is defined by $\mathbf{G}=[(\mathbf{a}^*(\phi_1)\otimes\mathbf{a}(\phi_1)),\cdots,(\mathbf{a}^*(\phi_K)\otimes\mathbf{a}(\phi_K))]$.

Being similar to the estimation of elevation, the model in equation (29) can be transformed into

$$\mathbf{r}_x=\mathbf{G}(\mathbf{\Phi})\tilde{\mathbf{q}}+\bar{\mathbf{n}}_x \tag{30}$$

where $\tilde{\mathbf{q}}$ is a sparse vector with the sparse level K, $\mathbf{\Phi}=(\phi_1,\cdots,\phi_D)$ with spacing $\Delta\phi$ in the range of interest. Since the number of sources is estimated in the previous subsection, the OMP with the refining grid step or the SPICE algorithms can be used to estimate the azimuth from equation (30). For the SPICE, the sparse vector $\tilde{\mathbf{q}}$ can be obtained by solving the following l_1-norm constraint optimization problem

$$\underbrace{\arg\min}_{\tilde{\mathbf{q}}}(\|\mathbf{r}_x-\mathbf{G}(\mathbf{\Phi})\tilde{\mathbf{q}}\|_2+\|\mathbf{D}\tilde{\mathbf{q}}\|_1) \tag{31}$$

where

$$\mathbf{D}=\mathrm{diag}\left(\frac{\|\mathbf{a}^*(\phi_1)\otimes\mathbf{a}(\phi_1)\|_2}{Q},\cdots,\frac{\|\mathbf{a}^*(\phi_D)\otimes\mathbf{a}(\phi_D)\|_2}{Q}\right) \tag{32}$$

Equation (31) can be interpreted as a weighted hyperparameter-free square-root LASSO, which obviates the need for selecting or tuning critical hyperparameters to strike a balance between data fidelity and sparsity. Thus, the azimuth $(\hat{\phi}_1,\cdots,\hat{\phi}_K)$ can be obtained by using the indices corresponding with the nonzero elements of the sparse vector $\tilde{\mathbf{q}}$.

3.3. Automatic pairing and estimation of Stokes parameters

Employing $(\hat{\phi}_1,\cdots,\hat{\phi}_K)$ and $(\hat{\theta}_1,\cdots,\hat{\theta}_K)$ obtained from the previous subsection, we form a 2-D grid set $\Upsilon(\theta,\phi)=\{(\hat{\theta}_1,\hat{\phi}_1),\cdots,(\hat{\theta}_1,\hat{\phi}_K),\cdots,(\hat{\theta}_K,\hat{\phi}_1),\cdots,(\hat{\theta}_K,\hat{\phi}_K)\}$. By the 2-D grid set $\Upsilon(\theta,\phi)$ with K^2 pair $(\hat{\theta},\hat{\phi})$, the model in equation (16) can be transformed into

$$\mathbf{r}=\mathbf{A}(\Upsilon)\tilde{\mathbf{e}}+\bar{\mathbf{n}} \tag{33}$$

The $4D \times 1$ block-sparse vector $\tilde{\mathbf{e}}$ is defined as

$$\tilde{\mathbf{e}} = [\bar{\mathbf{e}}_1^T, \bar{\mathbf{e}}_2^T, \cdots, \bar{\mathbf{e}}_D^T]^T \tag{34}$$

where $D = K^2$ and the ith 4×1 block vector $\bar{\mathbf{e}}_i = [e_{i_1}, e_{i_2}, e_{i_3}, e_{i_4}]^T$ $(i = 1, \cdots, D)$. Since the $4D \times 1$ block-sparse vector $\tilde{\mathbf{e}}$ has only K block vector with nonzero elements, $\tilde{\mathbf{e}}$ has the sparse level K.

The block sparse vector $\tilde{\mathbf{e}}$ can be obtained by solving the following l_2/l_1 minimization problem [32]

$$\underbrace{\arg\min}_{\bar{\mathbf{e}}_1, \cdots, \bar{\mathbf{e}}_D} \sum_{k=1}^{D} \|\bar{\mathbf{e}}_k\|_2 \;\; s.t. \|\mathbf{r} - \mathbf{A}(\Upsilon)\tilde{\mathbf{e}}\|_2 \le \nu \tag{35}$$

where ν bounds the l_2-norm of the noise in measurements. The equation (35) can be written into Square-Root LASSO problem [37], i.e.

$$\underbrace{\arg\min}_{\bar{\mathbf{e}}_1, \cdots, \bar{\mathbf{e}}_D} \|\mathbf{r} - \mathbf{A}(\Upsilon)\tilde{\mathbf{e}}\|_2 + \lambda \sum_{k=1}^{D} \|\bar{\mathbf{e}}_k\|_2 \tag{36}$$

where λ is the regularization parameter, which depends on the structure of the noise. Using convex programming tools [33], the equation (36) can be solved efficiently and this solution is referred to as convex solution (CVS). Thus, Stokes parameters of the received sources can be estimated by the K maximum elements in $\|\bar{\mathbf{e}}_k\|_2$, $(k = 1, \cdots, D)$, which are obtained from the convex solution of equation (36). The pair of 2-D DOAs $(\hat{\theta}_k, \hat{\phi}_k,\ k = 1, \cdots, K)$ can be obtained by using the indices of K maximum elements. But, the sparsity of the convex solution is determined by λ. In general, a large λ can induce more sparse solution, but it may incur solution bias [38]. To guarantee the better pair of 2-D DOAs, a large λ is required. Thus, there are large bias in estimating Stokes parameters by using CVS. In order to improve the performance, Stokes parameters of polarized sources are re-estimated by using LS and TLS, in the case of known pair $(\hat{\theta}, \hat{\phi})$. It is noted that Stokes parameters and 2-D DOAs of polarized sources may be estimated by solving the l_2/l_1 minimization problem, after we discretize the 2-D (θ, ϕ) plane as a uniform grid $\Upsilon(\theta, \phi) = \{(\theta_1, \phi_1), \cdots, (\theta_1, \phi_D), \cdots, (\theta_D, \phi_1), \cdots, (\theta_D, \phi_D)\}$ with spacing $\Delta\theta$ and $\Delta\phi$. But, there are many difficulties in implementation. First difficulty is that the computational complexity is very expensive. In general, the grid should not be too rough to achieve better precision. If the grid is too fine, however, the computational burden grows dramatically and the correlation between the columns of dictionary matrix increases. For example, if we take the grid set with step size 1° in −90° to 90°, the dictionary matrix in the 2-D (θ, ϕ) plane has 181^2 columns. As a result, the computing cost is very expensive for the l_2/l_1 minimization method. Second difficulty is that the number of sources must be known. Because the bounds between nonzero elements and zero elements in the block sparse vector is not clear due to the influence of noise, the number of sources can not be confirmed. The approach proposed in this paper can overcome these difficulties, so that it has better estimate performance.

4. CRB for polarized sources

The CRB is a lower bound on the estimation error variance for any unbiased estimator. Here, we derive the stochastic CRB for the 2-D DOAs and Stokes parameters of the polarized sources.

Under the aforementioned assumption, there is the following covariance matrix of the array output,

$$\mathbf{R} = \mathbf{\Psi}\mathbf{P}\mathbf{\Psi}^H + \sigma_n^2\mathbf{I} \tag{37}$$

where $\mathbf{P}$ is the $2K \times 2K$ covariance matrix of the polarized sources, i.e. $\mathbf{P} = \mathrm{diag}(\mathbf{R}_{E_1E_1}, \cdots, \mathbf{R}_{E_KE_K})$, the σ_n^2 is assumed to be known and the $2Q \times 2K$ steering matrix $\mathbf{\Psi} = [\mathbf{\Lambda}_1\mathbf{\Psi}_1, \cdots, \mathbf{\Lambda}_K\mathbf{\Psi}_K]$. Let $\mathbf{\Omega} = [\mathbf{\Theta}^T, \mathbf{\Phi}^T, \mathbf{g}^T]^T$ denote the unknown parameter vector, where $\mathbf{\Theta} = [\theta_1, \cdots, \theta_K]^T$, $\mathbf{\Phi} = [\phi_1, \cdots, \phi_K]^T$, $\mathbf{g} = [\bar{\mathbf{g}}_1, \cdots, \bar{\mathbf{g}}_K]^T$ with $\bar{\mathbf{g}}_k = [g_{0,k}, g_{1,k}, g_{2,k}, g_{3,k}]$. Under the previous assumption and Gaussian hypothesis, the Fisher information matrix (FIM) for the parameter vector $\mathbf{\Omega}$ is given in [34]:

$$\frac{1}{T}\mathrm{FIM} = \left(\frac{\partial \mathbf{V}}{\partial \mathbf{\Omega}^T}\right)^H \underbrace{\left(\mathbf{R}^{-T} \otimes \mathbf{R}^{-1}\right)}_{\mathbf{W}} \left(\frac{\partial \mathbf{V}}{\partial \mathbf{\Omega}^T}\right) = \mathbf{G}^H\mathbf{W}\mathbf{G} \tag{38}$$

where

$$\mathbf{V} = \mathrm{vec}(\mathbf{R}) = (\mathbf{\Psi}^* \otimes \mathbf{\Psi})\mathrm{vec}(\mathbf{P}) + \sigma_n^2\mathrm{vec}(\mathbf{I}) \tag{39}$$

$$\mathbf{G} = \left[\mathbf{G}_{\mathbf{\Theta}} \;\; \mathbf{G}_{\mathbf{\Phi}} \;\; \mathbf{G}_{\mathbf{g}}\right] = \left[\frac{\partial \mathbf{V}}{\partial \mathbf{\Theta}^T} \;\; \frac{\partial \mathbf{V}}{\partial \mathbf{\Phi}^T} \;\; \frac{\partial \mathbf{V}}{\partial \mathbf{g}^T}\right] \tag{40}$$

$$\frac{\partial \mathbf{V}}{\partial \mathbf{\Theta}^T} = \left[\frac{\partial(\mathbf{\Lambda}_1\mathbf{\Psi}_1)}{\partial\theta_1}\bar{\mathbf{e}}_1 \;\; \cdots \;\; \frac{\partial(\mathbf{\Lambda}_K\mathbf{\Psi}_K)}{\partial\theta_K}\bar{\mathbf{e}}_K\right] \tag{41}$$

$$\frac{\partial \mathbf{V}}{\partial \mathbf{\Phi}^T} = \left[\frac{\partial(\mathbf{\Lambda}_1\mathbf{\Psi}_1)}{\partial\phi_1}\bar{\mathbf{e}}_1 \;\; \cdots \;\; \frac{\partial(\mathbf{\Lambda}_K\mathbf{\Psi}_K)}{\partial\phi_K}\bar{\mathbf{e}}_K\right] \tag{42}$$

$$\frac{\partial \mathbf{V}}{\partial \mathbf{g}^T} = \left[(\mathbf{\Lambda}_1\mathbf{\Psi}_1)\frac{\partial \bar{\mathbf{e}}_1}{\partial \bar{\mathbf{g}}_1^T} \;\; \cdots \;\; (\mathbf{\Lambda}_K\mathbf{\Psi}_K)\frac{\partial \bar{\mathbf{e}}_K}{\partial \bar{\mathbf{g}}_K^T}\right] \tag{43}$$

Since $\mathbf{W}$ is positive definite and the $\mathrm{rank}(\mathbf{G}) \le \min\{6K, 4Q^2\}$ for the coprime array, it is clear that the FIM is nonsingular if and only if the $\mathrm{rank}(\mathbf{G}) = 6K$ when $6K \le 4Q^2$. Hence, if $K \le 2Q^2/3$, the FIM is invertible and the CRBs for $\mathbf{\Theta}$, $\mathbf{\Phi}$ and $\mathbf{g}$ are given by [35]

$$CRB(\mathbf{\Theta}) = \frac{1}{T}\left(\mathbf{G}_{\mathbf{\Theta}}^H\mathbf{W}^{1/2}\Pi^{\perp}_{\mathbf{W}^{1/2}\mathbf{G}_{\Phi g}}\mathbf{W}^{1/2}\mathbf{G}_{\mathbf{\Theta}}\right)^{-1} \tag{44}$$

$$CRB(\mathbf{\Phi}) = \frac{1}{T}\left(\mathbf{G}_{\mathbf{\Phi}}^H\mathbf{W}^{1/2}\Pi^{\perp}_{\mathbf{W}^{1/2}\mathbf{G}_{\Theta g}}\mathbf{W}^{1/2}\mathbf{G}_{\mathbf{\Phi}}\right)^{-1} \tag{45}$$

$$CRB(\mathbf{g}) = \frac{1}{T}\left(\mathbf{G}_{\mathbf{g}}^H\mathbf{W}^{1/2}\Pi^{\perp}_{\mathbf{W}^{1/2}\mathbf{G}_{\Theta\Phi}}\mathbf{W}^{1/2}\mathbf{G}_{\mathbf{g}}\right)^{-1} \tag{46}$$

where $\mathbf{G}_{\Phi g} = [\mathbf{G}_{\mathbf{\Phi}} \;\; \mathbf{G}_{\mathbf{g}}]$, $\mathbf{G}_{\Theta g} = [\mathbf{G}_{\mathbf{\Theta}} \;\; \mathbf{G}_{\mathbf{g}}]$, $\mathbf{G}_{\Theta\Phi} = [\mathbf{G}_{\mathbf{\Theta}} \;\; \mathbf{G}_{\mathbf{\Phi}}]$ and

$$\Pi^{\perp}_{\mathbf{W}^{1/2}\mathbf{G}_{\Phi g}} = \mathbf{I} - \mathbf{W}^{1/2}\mathbf{G}_{\Phi g}\left((\mathbf{W}^{1/2}\mathbf{G}_{\Phi g})^H\mathbf{W}^{1/2}\mathbf{G}_{\Phi g}\right)^{-1} \times (\mathbf{W}^{1/2}\mathbf{G}_{\Phi g})^H \tag{47}$$

$$\Pi^{\perp}_{\mathbf{W}^{1/2}\mathbf{G}_{\Theta g}} = \mathbf{I} - \mathbf{W}^{1/2}\mathbf{G}_{\Theta g}\left((\mathbf{W}^{1/2}\mathbf{G}_{\Theta g})^H\mathbf{W}^{1/2}\mathbf{G}_{\Theta g}\right)^{-1} \times (\mathbf{W}^{1/2}\mathbf{G}_{\Theta g})^H \tag{48}$$

$$\Pi^{\perp}_{\mathbf{W}^{1/2}\mathbf{G}_{\Theta\Phi}} = \mathbf{I} - \mathbf{W}^{1/2}\mathbf{G}_{\Theta\Phi}\left((\mathbf{W}^{1/2}\mathbf{G}_{\Theta\Phi})^H\mathbf{W}^{1/2}\mathbf{G}_{\Theta\Phi}\right)^{-1} \times (\mathbf{W}^{1/2}\mathbf{G}_{\Theta\Phi})^H \tag{49}$$

5. Monte Carlo simulations

In this section, we investigate the performance of the proposed algorithm by experiments. In each of the experiments, we generated 100 Monte Carlo runs. The signal-to-noise ratio (SNR) is equal to $10log_{10}(\sigma_s^2/\sigma_n^2)$ dB, where σ_s^2 and σ_n^2 are the signal and noise power, respectively. The CADiS with $M = 4$ and $N = 3$ is considered. This CADiS has two difference coarrays with different lags, as shown in Fig. 2. One (denoted by CADiS-1) has consecutive lags from $-12d$ to $12d$, the other (denoted by CADiS-2) has inconsecutive lags from $-15d$ to $15d$, where d taken as half of the wavelength. From −90° to 90°, we take the rough grid set with step size 1° and the fine grid set with step size 0.1°.

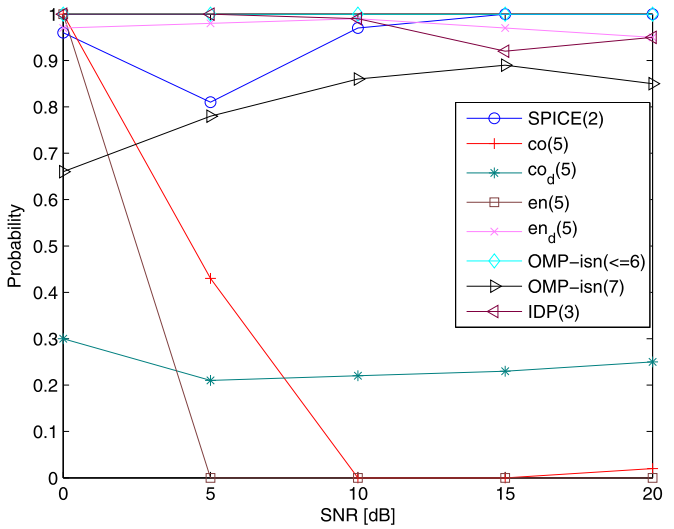

Fig. 3. Probability of detection versus SNR for different methods.

5.1. Detection performance

In this numerical experiment, we investigate the detection performance of finding the unknown number of sources for the BOMP-isn algorithm in case that CADiS-1 is employed, where the snapshots are 10000.

Besides the number of iteration is typically set to the sparsity level K of the sparse vector, there are several popular stopping rules for the OMP algorithm that can be implemented at minimal cost [36]: 1) Stop when the energy (or the change of energy) in the residual is small: $\|\mathbf{r}^k\|_2 \leq \epsilon$ or $(\|\mathbf{r}^{k-1}\|_2 - \|\mathbf{r}^k\|_2) \leq \epsilon$; 2) Stop when no column in the measurement matrix is strongly correlated with the residual or the change of correlation is small: $\|\mathbf{\Phi}^H\mathbf{r}^{k-1}\|_\infty \leq \epsilon$ or $(\|\mathbf{\Phi}^H\mathbf{r}^{k-1}\|_\infty - \|\mathbf{\Phi}^H\mathbf{r}^k\|_\infty) \leq \epsilon$. To compare the performance of detection, Fig. 3 gives the probability of detection versus SNR for the BOMP-isn, the OMP with these stopping rules, SPICE and interlaced double-precision (IDP) estimation algorithms, which do not require that the number of sources is known a priori. From Fig. 3, the probability of detection for OMP-isn algorithm (which is indicated by symbol OMP-isn (≤ 6) with $\varepsilon_0 = 37$) is equal to 1 from $SNR = 0$ dB to $SNR = 20$ dB, when the number of sources is less than 7. For the OMP algorithm with other stopping rules (which are indicated by symbols $en(5)$ with $\varepsilon_{en} = 8$, $en_d(5)$ with $\varepsilon_{en_d} = 2.8$, $co(5)$ with $\varepsilon_{co} = 750$ and $co_d(5)$ with $\varepsilon_{co_d} = 350$), the probability of detection is less than 1 for five sources, and when the number of sources is equal to 6, the probability of detection is 0. For the SPICE algorithm (which is indicated by symbol SPICE(2)), when the number of sources is unknown a priori, the probability of detection is less than 1 for two sources. For the IDP algorithm (which is indicated by symbol IDP(3)), the probability of detection is less than 1 for three sources. This implies that the OMP-isn is better than the OMP with other stopping rules in the ability to detect the number of sources. The reason is that the energy in the residual varies with SNR, so a fixed threshold is not found in a wide range of SNR. Similarly, the correlation between the column in the measurement matrix and the residual depends on SNR, so a fixed threshold is not found in a wide range of SNR. But the computational complexity for the OMP algorithm is less than that for the OMP-isn algorithm. The reason is that the OMP-isn algorithm requires an identifying step. The ability to detect the number of sources degrade for the SPICE and IDP algorithms. The reason is that there are the superfluous spectrum peaks in the spatial spectrum, which are mainly caused by the noise, for the IDP. Similarly, there are the superfluous nonzero elements in sparse solution, which are mainly caused by the regularization, for the SPICE.

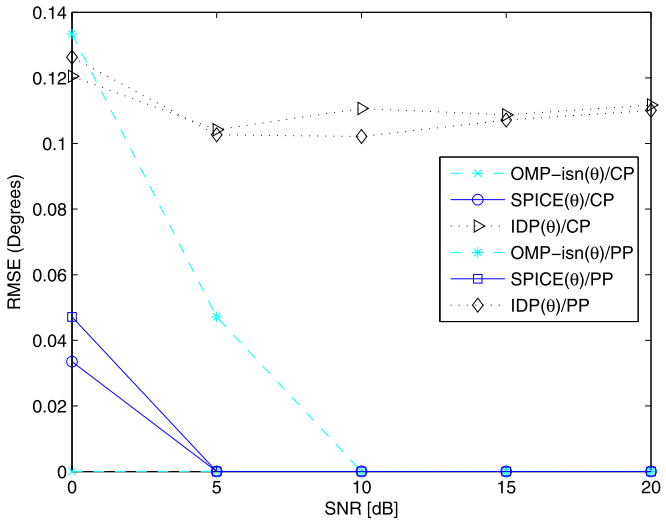

(a) the spacing $\delta = 1^\circ$ and CADiS-1

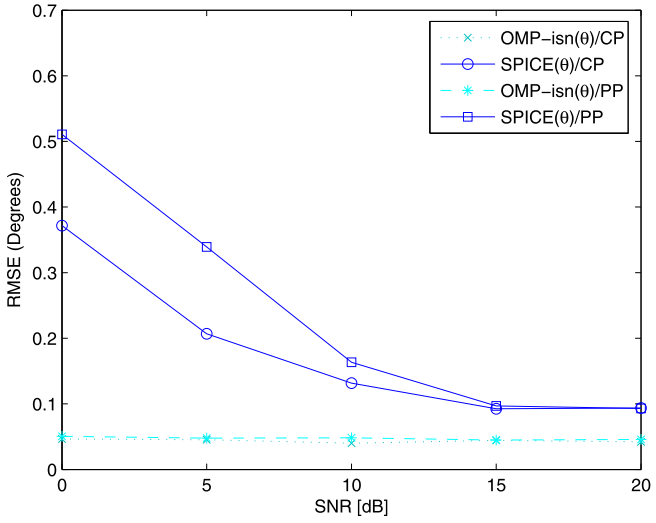

(b) the spacing $\delta = 0.1^\circ$ and CADiS-2

Fig. 4. The RMSE of elevation estimation versus SNR for three CP or PP sources.

5.2. Estimate performance for elevation

In this numerical experiment, we assess the performance of estimating elevation in case of three CP or PP sources. Stokes parameters of three CP sources are 1) $g_0 = 10.0$, $g_1 = -3.4$, $g_2 = 8.8$, $g_3 = 3.2$, $DP = 1$; 2) $g_0 = 10.0$, $g_1 = -6.4$, $g_2 = 2.6$, $g_3 = 7.1$, $DP = 1$; 3) $g_0 = 10.0$, $g_1 = -8.6$, $g_2 = 3.2$, $g_3 = 3.8$, $DP = 1$. Stokes parameters of three PP sources are 1) $g_0 = 13.2$, $g_1 = -6.7$, $g_2 = 6.9$, $g_3 = -4.0$, $DP = 0.78$; 2) $g_0 = 12.3$, $g_1 = -1.6$, $g_2 = 4.8$, $g_3 = -2.8$, $DP = 0.47$; 3) $g_0 = 11.3$, $g_1 = 3.3$, $g_2 = 2.7$, $g_3 = -1.6$, $DP = 0.40$. The RMSE of elevation estimation versus SNR for the OMP-isn, SPICE and IDP algorithms are given in Fig. 4, where snapshots are equal to 10000. In Fig. 4(a), the 2-D DOAs of three sources are 1) $\theta_1 = 75^\circ, \phi_1 = 70^\circ$, 2) $\theta_2 = 60^\circ, \phi_2 = 60^\circ$, 3) $\theta_3 = 40^\circ, \phi_3 = 50^\circ$, the spacing of grid is 1° and the CADiS-1 is used. In Fig. 4(b), the 2-D DOAs of three sources are 1) $\theta_1 = 45.3^\circ, \phi_1 = 80.8^\circ$, 2) $\theta_2 = 80.4^\circ, \phi_2 = 53.2^\circ$, 3) $\theta_3 = 63.6^\circ, \phi_3 = 68.3^\circ$, the spacing of grid is 0.1° and the CADiS-2 is used. From Fig. 4(a), the

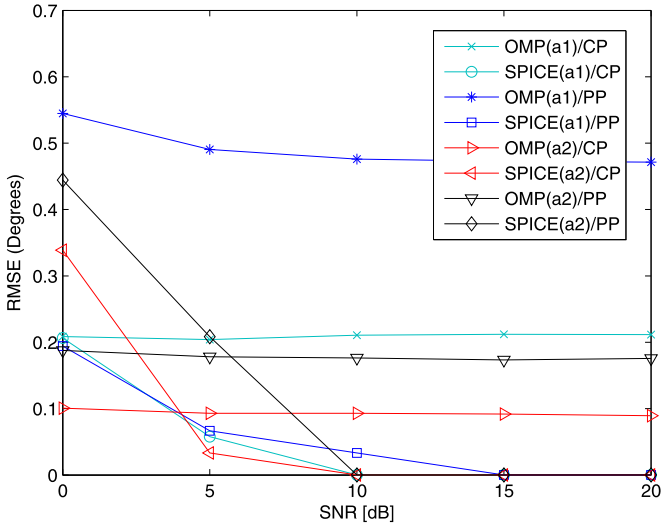

(a) the spacing $\delta = 1^\circ$

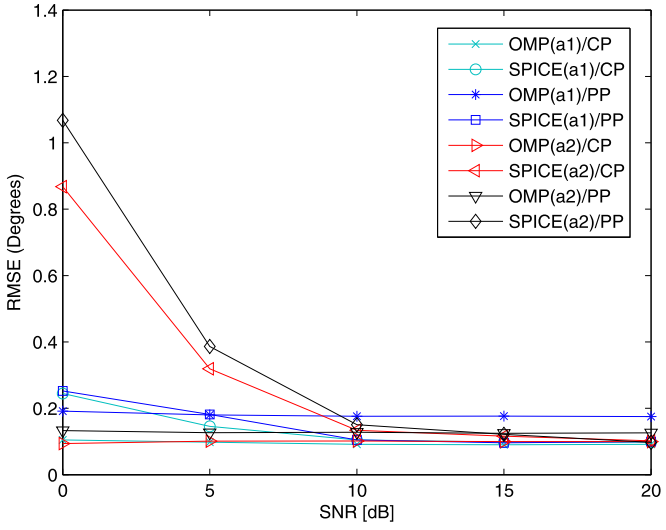

(b) the spacing $\delta = 0.1^\circ$

Fig. 5. The RMSE of azimuth estimation versus SNR for three CP or PP sources in case of CADiS-1 and CADiS-2.

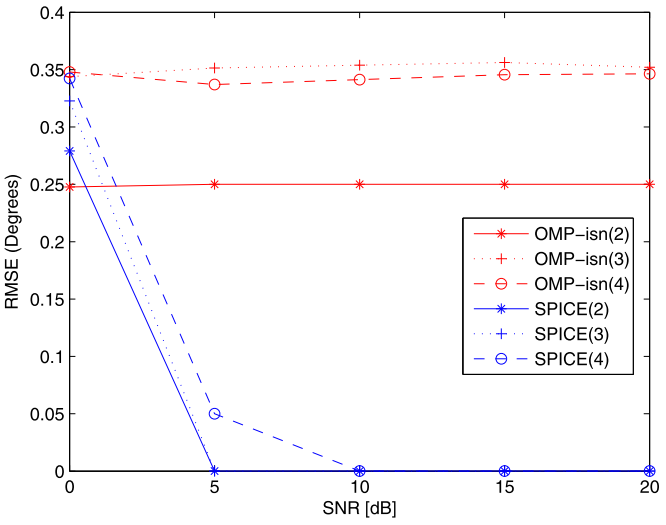

(a) Elevation θ

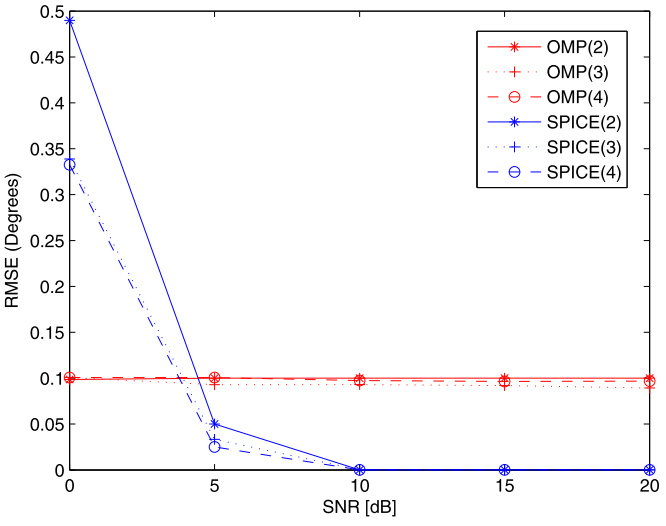

(b) Azimuth ϕ

Fig. 6. The RMSE of 2-D DOA estimation versus SNR for two, three and four CP sources in case of $\delta = 1^\circ$ and CADiS-2.

performance of the OMP-isn and SPICE is better than that of the IDP. For the OMP-isn, the RMSE of elevation estimation reaches to 0 when $SNR \geq 0$ dB for CP sources and when $SNR \geq 10$ dB for PP sources. The reason is that the OMP-isn algorithm can accurately recover the support of all K-sparse signals, when the SNR is more than a constant related with the isometry constant, the sparsity K and so on [36]. For the SPICE, the RMSE of elevation estimation reaches to 0 when $SNR \geq 5$ dB for CP and PP sources. But, the SPICE requires to know the number of sources. From Fig. 4(b), the performance of the OMP-isn is better than that of the SPICE. Since the CADiS-2 has some "holes" at ± 1, ± 14, the IDP fails in cases of CADiS-2.

5.3. Estimate performance for azimuth

In this numerical experiment, we assess the performance of estimating azimuth in case of three CP or PP sources and CADiS-1 or CADiS-2 are used. Stokes parameters of three CP sources are 1) $g_0 = 10.0, g_1 = 3.4, g_2 = 8.8, g_3 = 3.2, DP = 1$; 2) $g_0 = 10.0, g_1 = 6.4, g_2 = 2.6, g_3 = 7.2, DP = 1$; 3) $g_0 = 10.0, g_1 = 8.6, g_2 = 3.2, g_3 = 3.8, DP = 1$. Stokes parameters of three PP sources are 1) $g_0 = 10.6, g_1 = -3.3, g_2 = 4.8, g_3 = -2.8, DP = 0.61$; 2) $g_0 = 10.0, g_1 = 0, g_2 = 3.4, g_3 = -2.0, DP = 0.40$; 3) $g_0 = 10.3, g_1 = -1.6, g_2 = 4.1, g_3 = -2.4, DP = 0.49$. The RMSE of azimuth estimation versus SNR for the OMP, SPICE algorithms are given in Fig. 5, where snapshots are equal to 10000. In Fig. 5(a), the 2-D DOAs of three sources are 1) $\theta_1 = 45.3^\circ, \phi_1 = 70^\circ$, 2) $\theta_2 = 80.4^\circ, \phi_2 = 60^\circ$, 3) $\theta_3 = 63.6^\circ, \phi_3 = 50^\circ$ and the spacing of grid is 1°. In Fig. 5(b), the 2-D DOAs of three sources are 1) $\theta_1 = 45.3^\circ, \phi_1 = 80.8^\circ$, 2) $\theta_2 = 80.4^\circ, \phi_2 = 53.2^\circ$, 3) $\theta_3 = 63.6^\circ, \phi_3 = 68.3^\circ$ and the spacing of grid is 0.1°. From Fig. 5, the SPICE is better than OMP in case of high SNR ($SNR > 10$ dB) and rough grid (the spacing $\delta = 1^\circ$), and the RMSE can reach to 0. For SPICE, the RMSE of azimuth estimation increases along with the decrease of the spacing of grid. The reason is that the correlation between the columns of the measurement matrix increases. This results in the reduction of the recovery performance. For OMP, the RMSE of azimuth estimation keeps basically invariable from $SNR = 0$ dB to $SNR = 20$ dB and the performance using CADiS-2 is better than that using CADiS-1. The reason is that the OMP

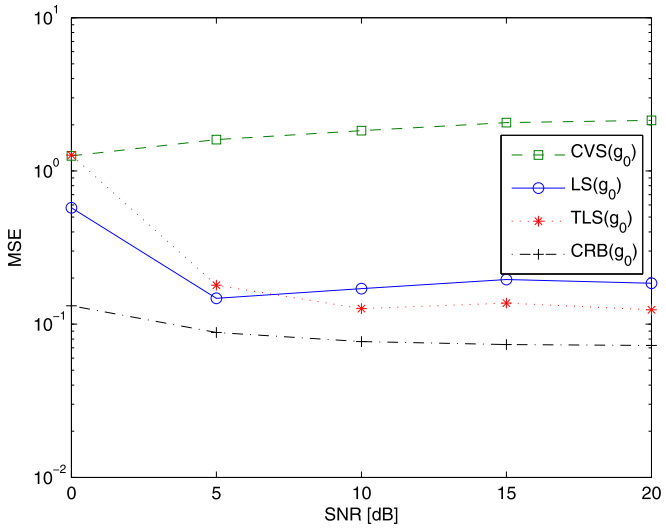

(a) Stokes parameter g_0

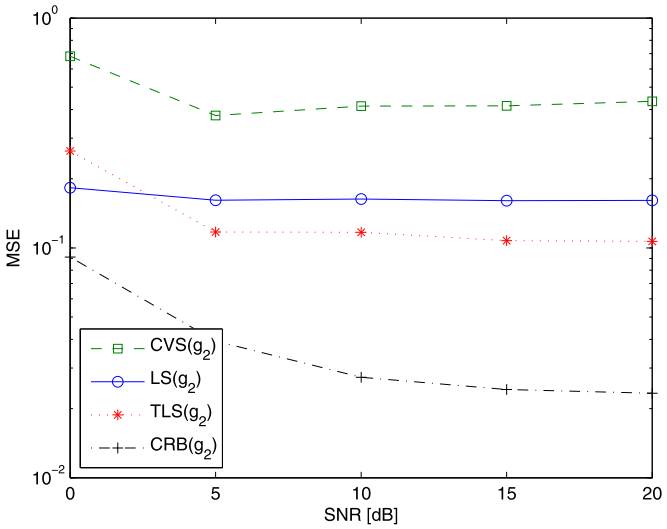

(c) Stokes parameter g_2

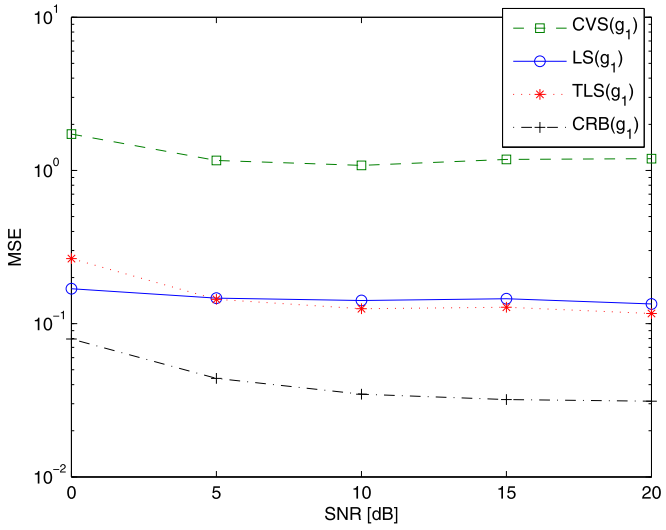

(b) Stokes parameter g_1

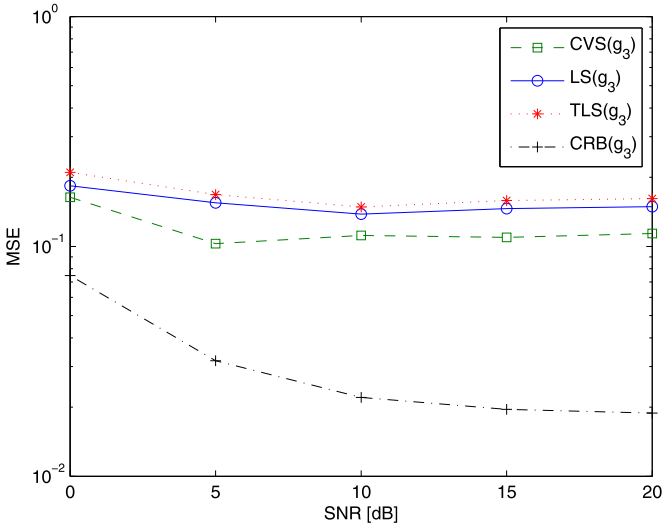

(d) Stokes parameter g_3

Fig. 7. The MSE of Stokes parameters estimation versus SNR for three CP sources in case of CADiS-1.

algorithm can recover the support of all K-sparse signals at an arbitrarily small but constant fraction of errors, when SNR, which is bounded, is more than a constant being dependent on the isometry constant [36]. The computational complexity for two approaches is compared in Table 2. From Table 2, the OMP is better than SPICE in the computational complexity.

When the number of sources changes, Fig. 6 shows the performance of the OMP-isn, OMP and SPICE algorithms in two, three and four CP sources, where the spacing of grid is 1°, the CADiS-2 is used and snapshots are equal to 10000. The 2-D DOAs of four sources are 1) $\theta_1 = 75°, \phi_1 = 70°$, 2) $\theta_2 = 67°, \phi_2 = 60°$, 3) $\theta_3 = 58°, \phi_3 = 50°$, 4) $\theta_4 = 47°, \phi_4 = 80°$. From Fig. 6, the SPICE is better than OMP-isn and OMP when $SNR \geq 5$ dB. For the SPICE and OMP, however, the number of sources must be known. For OMP-isn or OMP, the RMSE of elevation or azimuth estimation keep basically invariable from $SNR = 0$ dB to $SNR = 20$ dB. In addition, the RMSE of azimuth estimation for the OMP keep basically invariable along with the increase of sources' number. For the OMP-isn, however, the RMSE of two sources are less than that of three or four sources in the elevation estimation.

5.4. Estimate performance for Stokes parameters

In this numerical experiment, we assess the performance of estimating Stokes parameters in case of three CP or PP sources. The 2-D DOAs of three sources are 1) $\theta_1 = 45.3°, \phi_1 = 70°$, 2) $\theta_2 = 80.4°, \phi_2 = 60°$, 3) $\theta_3 = 63.6°, \phi_3 = 50°$. The effect of SNR on estimation performance is shown in Fig. 7 and 8, which snapshots are equal to 2000. In Fig. 7, three CP sources are considered and the CADiS-1 is used where Stokes parameters of three CP sources are 1) $g_0 = 12.0, g_1 = 4.1, g_2 = 10.6, g_3 = 3.86, DP = 1$; 2) $g_0 = 12.0, g_1 = 7.72, g_2 = 3.14, g_3 = 8.65, DP = 1$; 3) $g_0 = 12.0, g_1 = 10.4, g_2 = 3.86, g_3 = 4.6, DP = 1$. In Fig. 8, three PP sources are considered and the CADiS-2 is used, where Stokes parameters of three PP sources are 1) $g_0 = 13.24, g_1 = 6.69, g_2 = 6.89, g_3 = 3.99, DP = 0.78$; 2) $g_0 = 12.01, g_1 = 0.02, g_2 = 4.17, g_3 = 2.42, DP = 0.4$; 3) $g_0 = 12.65, g_1 = 3.38, g_2 = 5.54, g_3 = 3.2, DP = 0.57$. From Fig. 7 and 8, the performance of the LS and TLS is better than that of the CVS. The reason is that for the CVS, a large λ is required to guarantee the better pair of 2-D DOAs. Thus, the CVS has large bias in estimating Stokes parameters and belongs to *biased* estimator. The LS and TLS have almost identical

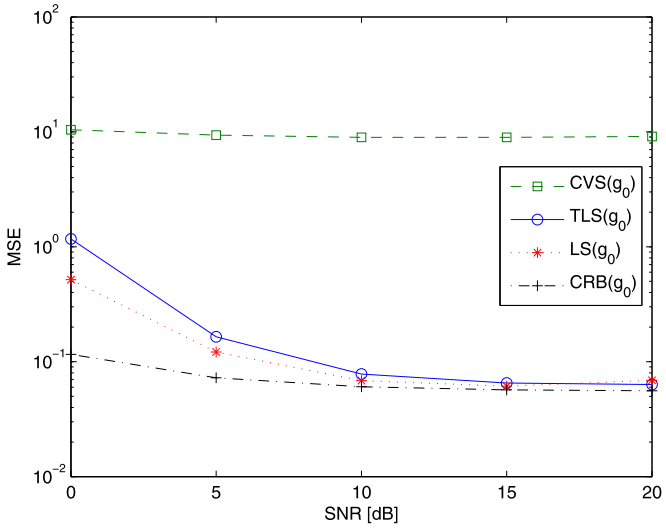

(a) Stokes parameter g_0

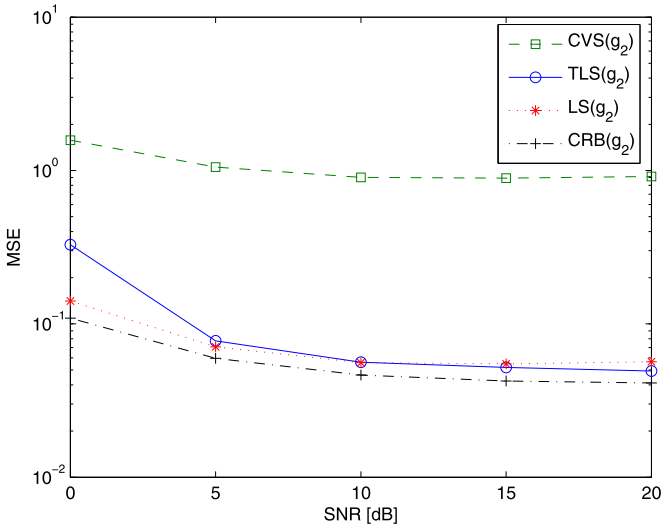

(c) Stokes parameter g_2

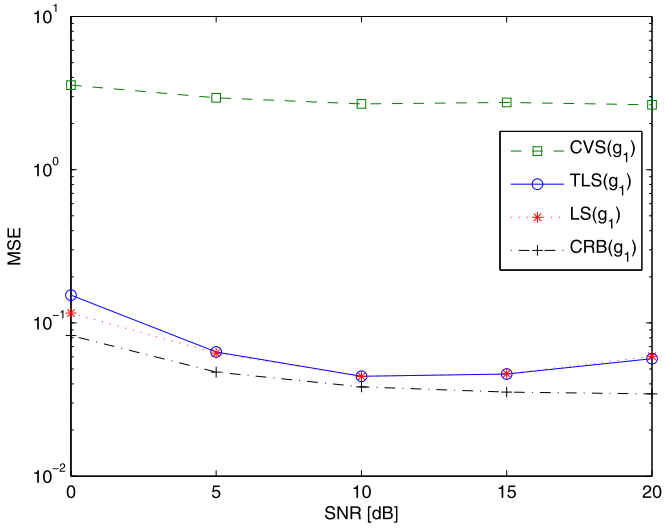

(b) Stokes parameter g_1

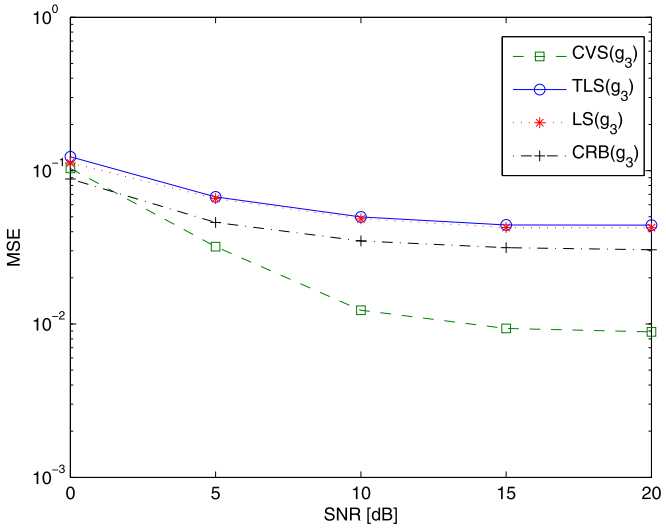

(d) Stokes parameter g_3

Fig. 8. The MSE of Stokes parameters estimation versus SNR for three PP sources in case of CADiS-2.

Table 2
The average run-times of each algorithm (unit:s).

the elevation estimation	OMP-isn	2.3×10^{-3}
	SPICE	306.8×10^{-3}
	IDP	16.1×10^{-3}
the azimuth estimation	OMP	1.2×10^{-3}
	SPICE (the spacing $\delta = 1°$)	295.9×10^{-3}
	SPICE (the spacing $\delta = 0.1°$)	943.1×10^{-3}
the pair of 2-D DOAs	CVS	376.6×10^{-3}
the Stokes parameters estimation	LS	0.13×10^{-6}
	TLS	1.7×10^{-3}

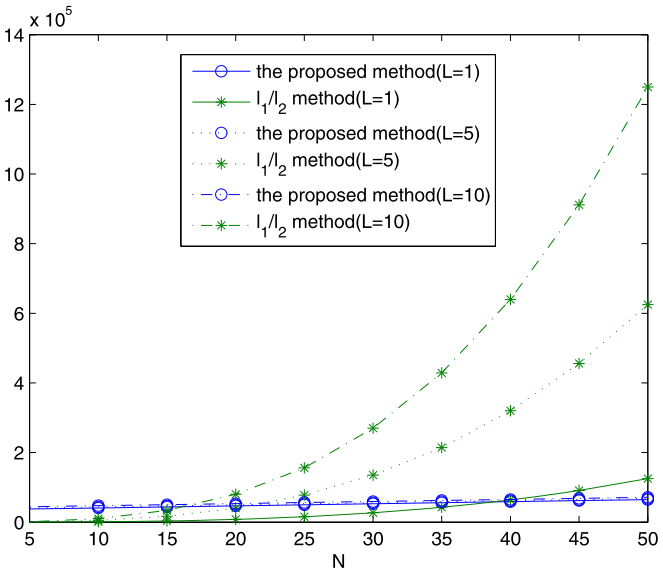

Fig. 9. Computational complexity versus the number of sampling grid.

performance. For PP sources, the MSE of estimating Stokes parameters are close to CRB in high SNR. But, the MSE of estimating Stokes parameters are far from CRB for CP sources. The reason is that the aperture of CADiS-1 is less than that of CADiS-2. In addition, the performance of 2-D DOA estimation can impact the performance of Stokes parameters estimation. It is noted that since the CVS is *biased* estimator, the CRB in this numerical experiment is only used to compare with the performance of the LS and TLS methods. Thus, it is possible that the MSE of the fourth Stokes parameter (g_3) estimation for the CVS is less than CRB.

5.5. Computational complexity analysis

The computational complexity for the OMP is in $O(NM + Mk + Mk^2 + k^3)$ at the kth iteration, where N denotes the number of sampling grid, M denotes the number of measurements and $N > M$ [32]. In case that the number of sources K is known, the iteration number of OMP is equal to K. Compared with the OMP, the computational complexity of BOMP-isn adds mainly $O(M^2)$ at the kth iteration due to the identifying step. Thus, the computational complexity for BOMP-isn is in $O(NM + Mk + Mk^2 + k^3 + M^2)$ at the kth iteration. In case that the number of sources K is unknown, however, the $K + 1$ iterations are only needed for the BOMP-isn. Since the SPICE batch algorithm and the CVS algorithm require repeated inversions of $N \times N$ matrices, each of which is of complexity $O(N^3)$ [30]. Thus, the computational complexity for the SPICE and CVS is mainly in $O(LN^3)$, where L is the number of iterations.

In Table 2, the average runtimes of different algorithms are given for scenarios corresponding to Fig. 4, Fig. 5, Fig. 7 and Fig. 8, respectively. The given runtimes are based on running the algorithms in MATLAB R2007a environment on a desktop computer with an Intel Core(TM)2 Duo CPU E7400 @2.8 GHz and 1.96 GB of RAM, and under the Microsoft Windows XP operating system. From Table 2, the computing cost for the OMP is minimum and the computing cost for the SPICE (the spacing $\delta = 0.1^\circ$) is maximum in elevation and azimuth estimation. This is consistent with the analysis in theory. In addition, the average runtime for the LS is only 0.13×10^{-6} (s). Comparing with the CVS, it is omitted.

When we take $M = 100$, $K = 3$ and $L = 1, 5, 10$, for example, the complexity for the proposed approach and the l_2/l_1 minimization method versus the number of sampling grid (N) is shown in Fig. 9. From Fig. 9, the complexity for the l_2/l_1 minimization method increases quickly along with the increase of N, but the complexity for the proposed approach (i.e. the sum of average runtimes of four algorithms: OMP-isn, OMP, CVS and LS) increases slowly. The complexity for the proposed approach is less than that for the l_2/l_1 minimization method, when $N \geq 40$ at $L = 1$, $N \geq 25$ at $L = 5$ and $N \geq 20$ at $L = 10$, respectively. In this paper, we take the grid set with step size 1° in -90° to 90°. Thus, the dictionary matrix in the 2-D (θ, ϕ) plane has 181^2 columns, i.e. $N = 181^2$. This renders that the computing cost is very expensive for the l_2/l_1 minimization method.

6. Conclusion

In this paper, a novel approach for estimating Stokes parameters and 2-D DOAs estimation of polarized sources is proposed based on the sparse reconstruction, in case of unknown number of sources. By analyzing the performances and complexities of the proposed approach, the following is summarized: 1) In elevation estimation, the OMP-isn is first chosen. After the number of sources is estimated, the SPICE may be chosen to reduce the RMSE of elevation estimation. 2) In azimuth estimation, the OMP is first chosen. In order to improve the performance of estimation, the SPICE may be chosen. 3) The pair of 2-D DOAs is implemented by CVS. In order to improve the accuracy of estimating Stokes parameters, the LS or TLS can be chosen. The proposed approach is suitable for both the CP and PP sources. The results of experiments show that the proposed approach has better performance.

Acknowledgments

This paper was supported by the National Natural Science Foundation of China under Grants 61571462.

References

[1] J. Li, R.T. Compton Jr., Angle and polarization estimation using ESPRIT with a polarization sensitive array, IEEE Trans. Antennas Propag. 39 (9) (1991) 1376–1383.
[2] J. Li, P. Stoica, D. Zheng, Efficient direction and polarization estimation with a COLD array, IEEE Trans. Antennas Propag. 44 (4) (1996) 539–547.
[3] K.T. Wong, M.D. Zoltowski, Uni-vector-sensor ESPRIT for multi-source azimuth, elevation, and polarization estimation, IEEE Trans. Antennas Propag. 45 (10) (1997) 1467–1474.
[4] K.T. Wong, M.D. Zoltowski, Self-initiating MUSIC direction finding & polarization estimation in spatio-polarizational beamspace, IEEE Trans. Antennas Propag. 48 (8) (2000) 1235–1245.
[5] A. Manikas, J.W.P. Ng, Crossed-dipole arrays for asynchronous DS-CDMA systems, IEEE Trans. Antennas Propag. 52 (1) (2004) 122–131.
[6] D. Rahamim, J. Tabrikian, R. Shavit, Source localization using vector sensor array in multipath environment, IEEE Trans. Signal Process. 52 (11) (2004) 3096–3103.
[7] H.S. Mir, J.D. Sahr, Passive direction finding using airborne vector sensors in the presence of manifold perturbations, IEEE Trans. Signal Process. 55 (1) (2007) 156–164.
[8] M. Hurtado, A. Nehorai, Performance analysis of passive low-grazing-angle source localization in maritime environments using vector sensors, IEEE Trans. Aerosp. Electron. Syst. 43 (2) (2007) 780–789.
[9] J. He, S. Jiang, J. Wang, Z. Liu, Polarization difference smoothing for direction finding of coherent signals, IEEE Trans. Aerosp. Electron. Syst. 46 (1) (2010) 469–480.
[10] J. Tao, L. Liu, Z. Lin, D.O.A. Joint, Range, and polarization estimation in the Fresnel region, IEEE Trans. Aerosp. Electron. Syst. 47 (4) (2011) 2657–2672.
[11] X. Guo, S. Miron, D. Brie, S. Zhu, X. Liao, A CANDECOMP/PARAFAC perspective on uniqueness of DOA estimation using a vector sensor array, IEEE Trans. Signal Process. 59 (7) (2011) 3475–3481.
[12] X. Yuan, Estimating the DOA and the polarization of a polynomial-phase signal using a single polarized vector-sensor, IEEE Trans. Signal Process. 60 (3) (2012) 1270–1282.
[13] X. Yuan, K.T. Wong, K. Agrawal, Polarization estimation with a dipole-dipole pair, a dipole-loop pair, or a loop-loop pair of various orientations, IEEE Trans. Antennas Propag. 60 (5) (2012) 2442–2452.
[14] M. Costa, V. Koivunen, A. Richter, DoA and polarization estimation for arbitrary array configurations, IEEE Trans. Signal Process. 60 (5) (2012) 2330–2343.

[15] Y. Tian, X.-Y. Sun, S.-S. Zhao, Sparse-reconstruction-based direction of arrival, polarisation and power estimation using a cross-dipole array, IET Radar Sonar Navig. 9 (6) (2015) 727–731.
[16] J. Li, P. Stoica, Efficient parameter estimation of partially polarized electromagnetic waves, IEEE Trans. Signal Process. 42 (11) (1994) 3114–3125.
[17] K.-G. Ho, K.-C. Tan, B.T.G. Tan, Efficient method for estimating directions-of-arrival of partially polarized signals with electromagnetic vector sensors, IEEE Trans. Signal Process. 45 (10) (1997) 2485–2498.
[18] J. He, M.O. Ahmad, M.N.S. Swamy, Near-field localization of partially polarized sources with a cross-dipole array, IEEE Trans. Aerosp. Electron. Syst. 49 (2) (2013) 857–870.
[19] K.T. Wong, X. Yuan, "Vector cross-product direction-finding" with an electromagnetic vector-sensor of six orthogonally oriented but spatially noncollocating dipoles/loops, IEEE Trans. Signal Process. 59 (1) (2011) 160–171.
[20] H. Tao, J. Xin, J. Wang, N. Zheng, A. Sano, Two-dimensional direction estimation for a mixture of noncoherent and coherent signals, IEEE Trans. Signal Process. 63 (2) (2015) 318–333.
[21] G. Wang, J. Xin, J. Wang, N. Zheng, A. Sano, Subspace-based two-dimensional direction estimation and tracking of multiple targets, IEEE Trans. Aerosp. Electron. Syst. 51 (2) (2015) 1386–1402.
[22] G. Niu, Y. Zhang, J. Guo, Interlaced double-precision 2-D angle estimation algorithm using L-shaped nested arrays, IEEE Signal Process. Lett. 23 (4) (2016) 522–526.
[23] Z. Cheng, Y. Zhao, Y. Zhu, P. Shui, H. Li, Sparse reconstruction based two-dimensional direction-of-arrival estimation method with L-shaped array, IET Radar Sonar Navig. 10 (5) (2016) 976–982.
[24] R.K. Raney, Dual-polarized SAR and Stokes parameters, IEEE Geosci. Remote Sens. Lett. 3 (3) (2006) 317–319.
[25] S.H. Yueh, W.J. Wilson, S.J. Dinardo, S.V. Hsiao, Polarimetric microwave wind radiometer model function and retrieval testing for WindSat, IEEE Trans. Geosci. Remote Sens. 44 (3) (2006) 584–596.
[26] J-W. Tao, Q-J. Fan, F. Yu, Stokes parameters and DOAs estimation of partially polarized sources using a EM vector-sensor, Signal Image Video Process. 11 (4) (2017) 737–744.
[27] S. Qin, Y.D. Zhang, M.G. Amin, Generalized coprime array configurations for direction-of-arrival estimation, IEEE Trans. Signal Process. 63 (6) (2015) 1377–1390.
[28] M. Yang, F. de Hoog, Orthogonal matching pursuit with thresholding and its application in compressive sensing, IEEE Trans. Signal Process. 63 (20) (2015) 5479–5486.
[29] P. Stoica, D. Zachariah, J. Li, Weighted SPICE: a unifying approach for hyperparameter-free sparse estimation, Digit. Signal Process. 33 (2014) 1–12.
[30] D. Zachariah, P. Stoica, Online hyperparameter-free sparse estimation method, IEEE Trans. Signal Process. 63 (13) (2015) 3348–3359.
[31] D. Malioutov, M. Cetin, A.S. Willsky, A sparse signal reconstruction perspective for source localization with sensor arrays, IEEE Trans. Signal Process. 53 (8) (2005) 3010–3022.
[32] M. Stojnic, F. Parvaresh, B. Hassibi, On the reconstruction of block-sparse signals with an optimal number of measurements, IEEE Trans. Signal Process. 57 (8) (2009) 3075–3085.
[33] M. Grant, S. Boyd, Cvx User's Guide for cvx Version 1.2 [On-line], Available: http://www.stanford.edu/boyd/software.html.
[34] P. Stoica, E.G. Larsson, A.B. Gershman, The stochastic CRB for array processing: a textbook derivation, IEEE Signal Process. Lett. 8 (5) (2001) 148–150.
[35] A. Koochakzadeh, P. Pal, Cramer–Rao bounds for underdetermined source localization, IEEE Signal Process. Lett. 23 (7) (2016) 919–923.
[36] J. Wang, Support recovery with orthogonal matching pursuit in the presence of noise, IEEE Trans. Signal Process. 63 (21) (2015) 5868–5877.
[37] A. Belloni, V. Chernozhukov, L. Wang, Square-root LASSO: pivotal recovery of sparse signal via conic programming, Biometrika 98 (4) (2011) 791–806.
[38] M. Tan, I.W. Tsang, L. Wang, Matching pursuit LASSO part I: sparse recovery over big dictionary, IEEE Trans. Signal Process. 63 (3) (2015) 727–741.
[39] H.L. Van Trees, Optimum Array Processing, Johk Wiley and Sons. Inc. Press, New York, 2002.
[40] J. Wang, B. Shim, Exact recovery of sparse signals using orthogonal matching pursuit: how many iterations do we need?, IEEE Trans. Signal Process. 64 (16) (2016) 4194–4202.

Wen-xiu Chang received her B.S. degree in electronic engineering from Jilin University of Technology, Changchun, China, in 1982. She is currently with College of Communication Engineering, Jilin University, China, where she is a professor.

Her research interests include statistical signal processing and electromagnetic measurement.

Xin-bo Li received his Ph.D. degree in communication engineering from Jilin University, Changchun, China, in 2008. He is currently with College of Communication Engineering, Jilin University, China, where he is an associate professor.

His research interests include statistical signal processing and array signal processing.

Jun Wang is now reading for her B.S. degree in communication engineering from Jilin University, Changchun, China.

Her research interests include statistical signal processing.